Anti-trapping of indirect excitons by a current filament

2007 J. Phys.: Condens. Matter 19 295215

(http://iopscience.iop.org/0953-8984/19/29/295215)

IOP PUBLISHING JOURNAL OF PHYSICS: CONDENSED MATTER

J. Phys.: Condens. Matter **19** (2007) 295215 (10pp) doi:10.1088/0953-8984/19/29/295215

Anti-trapping of indirect excitons by a current filament

L Mouchliadis and A L Ivanov

Department of Physics and Astronomy, Cardiff University, Cardiff CF24 3AA, UK

E-mail: mouchliadisl@cf.ac.uk

Received 17 April 2007
Published 11 June 2007
Online at stacks.iop.org/JPhysCM/19/295215

Abstract

In order to explain the photoluminescence (PL) of indirect excitons collected from localized spots in experiments with a defocused laser excitation of coupled quantum wells (QWs), we model the in-plane carrier transport and charge distribution with a set of drift-diffusion, Poisson and thermalization equations. The quantum statistical corrections are included in our description via a generalized Einstein relationship and quantum mass action law. The PL spots are attributed to transverse current filaments crossing the structure and injecting electrons in the coupled QWs. The accumulated electron charge forms an anti-trap for indirect excitons. Our model quantitatively reproduces the whole set of the relevant experimental data.

1. Introduction

Excitons are the lowest-lying excitations in solids, and in the dilute limit they behave as bosons since they consist of two fermions, an electron and a hole. In GaAs/AlGaAs coupled quantum wells under applied bias, electrons and holes tend to be trapped in different wells, and therefore the overlap of their wavefunctions decreases. As a result, an indirect exciton with a long lifetime is formed, since the spatial separation suppresses the electron–hole recombination.

Recently a nearly symmetric pattern of two concentric photoluminescence rings associated with indirect excitons has been reported, when double quantum well structures are illuminated by a tightly focused laser which induces the interband transitions [1–3]. According to one of these reports [1], the external ring is fragmented in a periodic array of PL spots as the temperature is lowered. Moreover, inside the area defined by the external ring several randomly distributed PL centres (PLCs) appear, and their number increases with increasing applied voltage. Since in these experiments the laser energy is tuned above the AlGaAs barrier energy, the generation of free carriers is significant. The origin of the external ring has already been clarified in terms of a dynamical p–n junction, where electrons and holes are dominant in different in-plane regions and excitons are formed only in the interface between these two regions [4–7]. The inner ring has also been explained: the photoexcited indirect excitons are hot, but as they diffuse away from the excitation spot they cool down and become optically active, giving rise to a local increase of the PL signal [8, 9]. In contrast to the PL rings, there has been no theoretical model describing the PL centres. The PLCs are characterized by (i)

an in-plane fixed position (spatial pinning of the PL spots associated with the PLCs), (ii) a 'Mexican hat' structure of the spatially resolved photoluminescence signal, and (iii) a bell-like shape of the blue shift of the PL line [10–12]. In this paper we explain and model the PL centres by using a drift-diffusion equation for the in-plane carrier transport, a Poisson equation for the charge accumulated in the coupled QWs, and a thermalization equation for electrically injected and photo-injected carriers. The quantum-statistical corrections are included in the description, although they are not crucially important for the explanation of the experimental data.

The underlying physics of our model is the following one. The PLCs originate from the current filaments crossing the coupled QWs [6, 7]. Thus, in the vicinity of these defects, charge accumulates as a part of electrons from the filament are captured in the wells and a repulsive potential for electrons and indirect excitons is created. The drift force resulting from this potential induces the in-plane electron transport away from the centre of the filament. However, the photogenerated holes undergo an attraction from the negatively charged area around the filament and move towards it. As the holes encounter the outward-moving electrons they bind to form excitons which then decay and give rise to the PL signal. The repulsive potential around the filament acts as an *anti-trap* for the dense electron gas, as well as for the secondary created indirect excitons. Note that although trapping of excitons has already been studied in various works [13–18], this is the first time that the influence of an anti-trapping, repulsive potential has been considered. Excitons around the filament are scarce, due to an effective heating by the transverse filament current, and only at a distance of approximately 10 μm from the PLCs does an exciton cloud effectively form. Far from this cloud the excitonic gas becomes dilute again, due to a small concentration of electrons. The local increase of the excitonic energy originates from the anti-trapping character of the in-plane potential around the filament.

The most important feature of the PLCs, where an electrical breakdown occurs, is that electrons are dominant and their concentration can be visualized as a blue shift of the PL spectrum. Thus, in our model the laser-generated electrons and holes, as well as the secondary excitons, are 'probe particles', while the main effect is due to the electric current induced heating and accumulated charge. With increasing applied voltage the number of the localized spots increases, indicating that the current flowing through the wells becomes significant. Furthermore, the electrons, which are injected in the wells by the transverse electric filament, are hot at the anti-trap centres. This suppresses both the indirect exciton formation and the excitonic photoluminescence signal. As the electrically injected electrons move away from the anti-trap centre, they cool down, giving rise to indirect excitons, and therefore to the PL signal. Thus, the picture we propose explains both the 'Mexican hat' shape of the PL signal and the bell-like profile of the shift of the PL line.

In section 2 we present the drift-diffusion and Poisson equations used in the model and describe the formation of excitons through a quantum mass action law. The longitudinal acoustic (LA)-phonon-assisted relaxational thermodynamics of electrons is described and a thermalization equation is derived. In section 3 the main results of the model are discussed and compared with the experimental data. Finally, section 4 summarizes our conclusions.

2. Model

2.1. Drift-diffusion

In our model a PLC is due to a transverse current filament crossing the coupled QW structure and creating a local in-plane source of QW electrons. In the vicinity of the source, an effective repulsive potential is created for electrons, as the negative charge builds up around it. The accumulation of charge results in in-plane diffusion and drift of the electrons. The electrically induced charge, trapped by the coupled QWs, creates a potential U_{Coulomb} which influences the

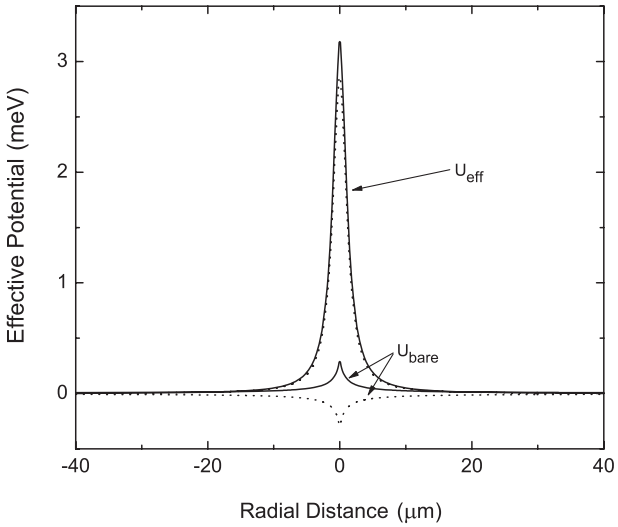

Figure 1. The anti-trap profile is plotted as a function of the radial distance from the filament centre for repulsive (solid line) and attractive (dotted line) bare potentials. The corresponding bare potentials are also shown. The parameters used are $\alpha_0 = \pm 1.2$ meV μm^2 and $r_0 = 2$ μm.

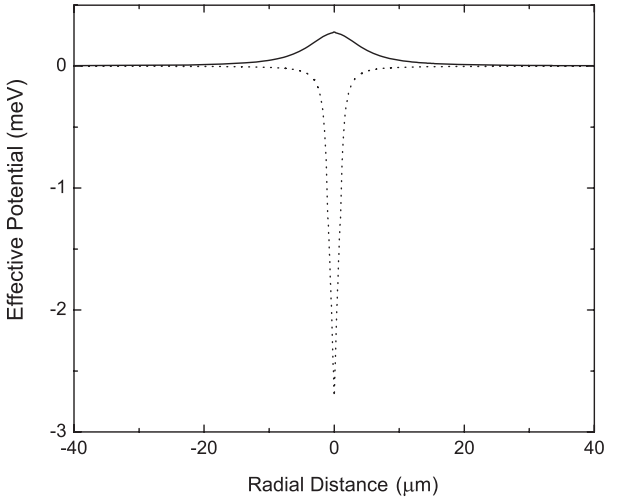

Figure 2. The effective potential $U_{\rm eff}$ against the radial distance from the filament centre. In the presence of a very deep attractive bare potential (dotted line) the effective potential (solid line) remains repulsive, although it becomes less steep and broader. The parameters used for the bare potential are $\alpha_0 = -2.75$ meV μm^2 and $r_0 = 1$ μm.

transport of carriers and the formation of excitons. The potential of accumulated electrons is given by Poisson's equation, and the bare input potential $U_{\rm bare} = \alpha_0/(r^2 + r_0^2)$, where α_0 and r_0 are fitting parameters. For numerical calculations we use $\alpha_0 = 1.2$ meV μm^2 and $r_0 = 2$ μm. However, the overall repulsive character of the effective potential is not strongly affected by the bare potential, as shown in figures 1 and 2. The effective potential is the sum of these two contributions, $U_{\rm eff} = U_{\rm bare} + U_{\rm Coulomb}$.

Around the filament the electron density is high, and steep gradients in the concentration exist. Under the influence of both drift and diffusion forces, the electronic gas expands in the QW plane, as is shown in figure 3. The system of drift-diffusion and Poisson equations we use to model the PLCs is given by

$$\frac{\partial n_{2\rm d}^{\rm e}}{\partial t} = \nabla_{2\rm d}\left[D_{\rm e}\nabla_{2\rm d} n_{2\rm d}^{\rm e} + \mu_{\rm e} n_{2\rm d}^{\rm e}\nabla_{2\rm d} U_{\rm eff}^{\rm e}\right] - \gamma n_{2\rm d}^{\rm e} n_{2\rm d}^{\rm h} + \Lambda^{\rm e} + \Lambda_0^{\rm e}, \tag{1}$$

$$\frac{\partial n_{2\rm d}^{\rm h}}{\partial t} = \nabla_{2\rm d}\left[D_{\rm h}\nabla_{2\rm d} n_{2\rm d}^{\rm h} + \mu_{\rm h} n_{2\rm d}^{\rm h}\nabla U_{\rm eff}^{\rm h}\right] - \gamma n_{2\rm d}^{\rm e} n_{2\rm d}^{\rm h} + \Lambda^{\rm h}, \tag{2}$$

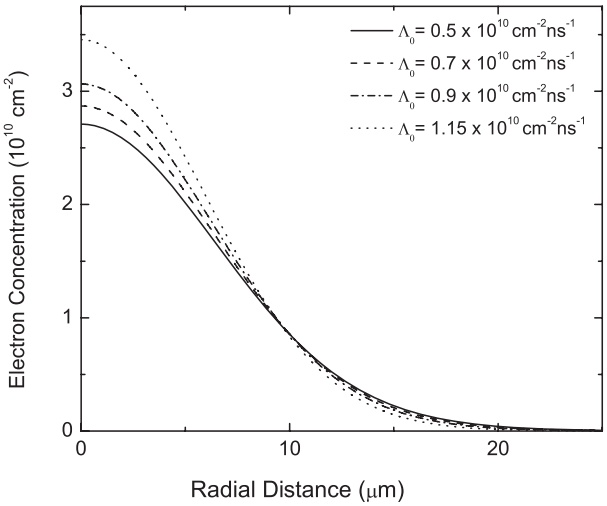

Figure 3. The electron concentration as a function of the radial distance from the anti-trap centre for four different generation rates.

$$\nabla_{3d}^2 U_{\text{Coulomb}} = -\frac{e^2 n_{2d}^{e}}{\varepsilon_b}, \tag{3}$$

$$U_{\text{eff}}^{e} = U_{\text{bare}} + U_{\text{Coulomb}}; \qquad U_{\text{eff}}^{h} = u_0 n_{2d}^{e}, \tag{4}$$

where $\nabla_{2d} = \mathbf{e}_x \partial/\partial x + \mathbf{e}_y \partial/\partial y$, $\nabla_{3d} = \nabla_{2d} + \mathbf{e}_z \partial/\partial z$ (the z-axis is normal to the structure), and the mobilities are

$$\mu_{e(h)} = \frac{D_{e(h)}}{k_B T_0^{e(h)}} \left(1 - e^{-T_0^{e(h)}/T}\right). \tag{5}$$

In equations (1)–(4), $D_{e(h)}$ and $n_{2d}^{e(h)}$ are the diffusion coefficient and two-dimensional concentration of electrons (holes), respectively, e is the free-electron charge, k_B is Boltzmann's constant and ε_b is the background dielectric constant. The amplitude u_0 of the dipole–dipole interaction can be well approximated by the plate capacitor formula, $u_0 = 2\pi(e^2/\varepsilon_b)d$, with d the separation between the electron and hole layers [19]. In equation (5), T is the effective temperature of QW carriers and excitons, and $T_0^{e(h)}$ is the QW electron (hole) degeneracy temperature.

The mobilities are related to the diffusion coefficients via the generalized Einstein relationship for quasi-two-dimensional fermions, equation (5), which reduces to the usual one in the classical limit $T \gg T_0^{e(h)}$. A similar relationship was derived earlier for quasi-two-dimensional bosons (excitons) [20, 21]. The quantum corrections are incorporated in the equations through the degeneracy temperatures:

$$k_B T_0^{e(h)} = \frac{\pi \hbar^2}{m_{e(h)}} n_{2d}^{e(h)}, \tag{6}$$

where $m_{e(h)}$ is the in-plane effective mass of electrons (holes).

The nonlinear term on the right-hand side of equations (1) and (2) is proportional to the product of the electron and hole concentrations, and it describes the radiative recombination of bound and unbound electron–hole pairs. The capture coefficient γ corresponds to a time of a few picoseconds and has been calculated within a microscopic approach [22]. Note that although the transport is quasi-two-dimensional, the Poisson equation has to be solved in three dimensions.

The generation rates of electrons and holes, due to the optical pump, are given by Λ^h and Λ^e, whereas the rate Λ_0^e refers to electrons from the filament which are captured in the wells.

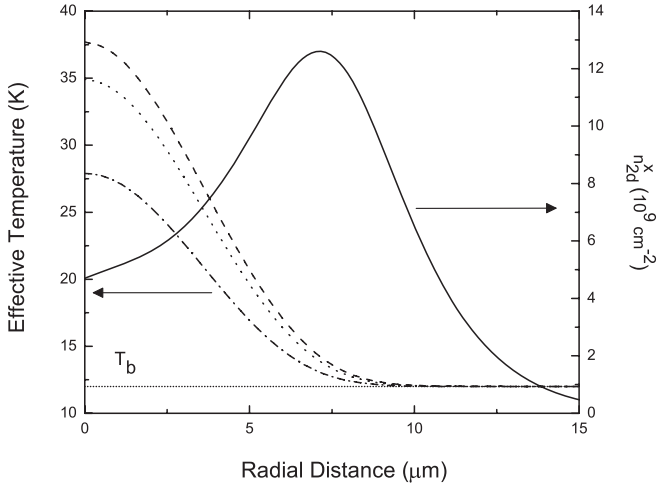

Figure 4. The effective temperature as a function of the radial distance from the anti-trap centre, for three different generation rates. The electronic gas is heated by the electric current and photocurrent and reaches the bath temperature 12 K in a distance of about 10 μm. The concentration of secondary excitons, $n^{\mathrm{x}}_{2\mathrm{d}}$, calculated with equation (9) is shown by the solid line. As the temperature falls with increasing $r_{\|}$, the exciton concentration reaches a maximum.

For numerical simulations we take $\Lambda^{\mathrm{h}} = \Lambda^{\mathrm{e}}$, and neglect diffusion of holes since under a defocused excitation the photogenerated carriers are scarce.

Equations (1)–(3) define the in-plane carrier transport, and they are solved numerically in order to model the experimental data. The only input fitting parameter used in numerical simulations is the carrier generation rate, which is inferred from the electric current measurements [12]. Note that in our model the indirect excitons appear as secondary particles in a rather small ring-shaped area around the filament (see figure 4) and therefore practically do not contribute to the thermalization and diffusion processes.

2.2. Quantum mass action law

We calculate the concentration $n^{\mathrm{x}}_{2\mathrm{d}}$ of indirect excitons assuming that the quasi-two-dimensional electron, hole and exciton gases are in quasi-equilibrium:

$$\mathrm{x} \rightleftharpoons \mathrm{e} + \mathrm{h}. \tag{7}$$

This means that the chemical potentials of the three species satisfy the condition

$$\mu_{\mathrm{x}} = \mu_{\mathrm{e}} + \mu_{\mathrm{h}}. \tag{8}$$

Substituting the expressions for the chemical potentials, one obtains a quantum mass action law for the excitonic concentration:

$$n^{\mathrm{x}}_{2\mathrm{d}} = -\frac{2M_{\mathrm{x}}k_{\mathrm{B}}T}{\pi\hbar^2}\ln[1 - \mathrm{e}^{-E_{\mathrm{b}}/k_{\mathrm{B}}T}(\mathrm{e}^{T^{\mathrm{e}}_0/T} - 1)(\mathrm{e}^{T^{\mathrm{h}}_0/T} - 1)], \tag{9}$$

where E_{b} is the exciton binding energy and M_{x} is the in-plane exciton mass. In the classical limit, equation (8) reduces to the well-known Saha formula [23]:

$$n^{\mathrm{x}}_{2\mathrm{d}} = \frac{2\pi\hbar^2 M_{\mathrm{x}}}{m_{\mathrm{e}}m_{\mathrm{h}}k_{\mathrm{B}}T}\, n^{\mathrm{e}}_{2\mathrm{d}}\, n^{\mathrm{h}}_{2\mathrm{d}}\mathrm{e}^{-E_{\mathrm{b}}/k_{\mathrm{B}}T}. \tag{10}$$

Equation (8) allows us to calculate the concentration of excitons, which are secondary particles originating from the binding of free electrons and holes, by using the results of

the drift-diffusion model, equations (1)–(3). The exciton binding energy for GaAs is $E_b = 3.5$ meV [24], which corresponds to a temperature of approximately 40 K. At high laser excitations, the electronic gas around the filament has temperature $T \sim 20$–40 K (see figure 4). In this case, nearly all excitons are ionized, according to the mass action law, and only free electrons and holes exist around the filament. However, at a distance of 10 μm electrons reach the lattice temperature and the excitonic PL ring appears. The temperature change with the distance is described in the following subsection.

2.3. Thermalization

Electrically injected or photo-injected QW carriers are hot, and they cool down to the lattice temperature via LA-phonon emission. Thermalization of the particles injected in the coupled QWs is dominated by electrons, because around the filament $n^{e}_{2d} \gg n^{h}_{2d}, n^{x}_{2d}$. The underlying physical picture we use refers to the relaxational thermodynamics [25], and the electron–electron scattering is assumed to be more efficient than the interaction of electrons with bulk LA-phonons. In this case, which refers to $n^{e}_{2d} \gtrsim 10^9$ cm^{-2}, the thermalization occurs through the quasi-equilibrium thermodynamic states, characterized by an effective electron temperature T and concentration n^{e}_{2d} [21]. In our approach the confinement of phonons is neglected. This is a good approximation since the acoustical branches remain propagative and bulk-like. The starting point for the thermalization equation is the Boltzmann–Uhlenbeck equation:

$$\frac{\partial}{\partial t}N_{\mathbf{k}} = -\frac{2\pi}{\hbar}\sum_{\mathbf{q}}|W_q|^2\{[N^{e}_{\mathbf{k}}(1+n_{\mathbf{q}})(1-N^{e}_{\mathbf{k}-\mathbf{q}}) - (1-N^{e}_{\mathbf{k}})n_{\mathbf{q}}N^{e}_{\mathbf{k}-\mathbf{q}}] \times \delta(E_{\mathbf{k}} - E_{\mathbf{k}-\mathbf{q}} - \hbar q\upsilon_s) + [N^{e}_{\mathbf{k}}n_{\mathbf{q}}(1-N^{e}_{\mathbf{k}+\mathbf{q}}) - (1-N^{e}_{\mathbf{k}})(1+n_{\mathbf{q}})N^{e}_{\mathbf{k}+\mathbf{q}}] \times \delta(E_{\mathbf{k}} - E_{\mathbf{k}+\mathbf{q}} + \hbar q\upsilon_s)\}, \tag{11}$$

where $N^{e}_{\mathbf{k}}$ and $n_{\mathbf{q}}$ are the occupation numbers of electrons and phonons, respectively, and υ_s is the sound velocity associated with LA-phonons. The two terms in the square brackets on the right-hand side of equation (11) describe Stokes and anti-Stokes scattering processes. If we consider only electrons in the ground-state mode $\mathbf{k} = 0$, Stokes scattering is not allowed, and equation (11) reduces to

$$\frac{\partial}{\partial t}N_{\mathbf{k}=0} = -\frac{2\pi}{\hbar}\sum_{\mathbf{q}}|W_q|^2\{[N^{e}_{\mathbf{k}=0}n_{\mathbf{q}}(1-N^{e}_{\mathbf{q}}) - (1-N^{e}_{\mathbf{k}=0})(1+n_{\mathbf{q}})N^{e}_{\mathbf{q}}]\} \times \delta(\hbar q\upsilon_s - E_{\mathbf{k}+\mathbf{q}}), \tag{12}$$

where the matrix element of the interaction is given by

$$W(q) = \sqrt{\frac{\hbar q}{2\rho\upsilon_s V}}\, D_{dp}F_z\left(\frac{q_z L_z}{2}\right),$$

D_{dp} is the deformation potential for electrons, ρ is the crystal density, and the form-factor $F_z(x) = [\sin x/x][e^{ix}/(1-x^2/\pi^2)]$ refers to an infinite rectangular QW confinement potential and describes the relaxation of momentum conservation in the z-direction.

For the ground-state mode the occupation number is given by $N^{e}_{E=0} = 1 - e^{-T^{e}_0/T}$. By differentiating this with respect to time and using equation (12) rewritten in the energy basis, one derives

$$\left(\frac{\partial T}{\partial t}\right)_{2d} = -\frac{2\pi}{\tau_{sc}}\frac{T^2}{T^{e}_0}(e^{T^{e}_0/T}-1)\int_1^\infty d\varepsilon\,\varepsilon\sqrt{\frac{\varepsilon}{\varepsilon-1}}|F_z(\alpha\sqrt{\varepsilon(\varepsilon-1)})|^2 \times \left(\frac{e^{\varepsilon E_0/k_B T_b} - e^{\varepsilon E_0/k_B T}}{e^{\varepsilon E_0/k_B T_b} + e^{T^{e}_0/T} - 1}\right)\left(\frac{1}{e^{\varepsilon E_0/k_B T_b} - 1}\right) + S_{pump}, \tag{13}$$

where $\tau_{sc} = (\pi^2\hbar^4\rho/D_{dp}^2 m_e^3 \upsilon_s)$ is the characteristic scattering time and $E_0 = 2m_e\upsilon_s^2$ is a characteristic thermalization energy. Equation (13) describes the thermalization dynamics of electrons from the initial effective temperature $T_i = T(t = 0)$ to the bath temperature T_b. The effective cooling of electrons in the presence of a bath of thermal bulk phonons is due to the relaxation of momentum conservation in the z-direction, which results in the coupling of the ground-state mode $\mathbf{k} = 0$ to a continuum of states $E \geqslant E_0$ rather than the single energy state $E = E_0$ [21, 25].

The extra term S_{pump} is added to include the heating of electrons by the current filament and laser pulse. This term is

$$S_{pump} = \frac{(E_i - k_B T I_2)\Lambda_{T_0}}{2k_B T I_1 - k_B T_0 I_2}, \tag{14}$$

where $I_1 = \int_0^\infty dz[z/(Ae^z + 1)]$, $I_2 = (e^{T_0/T})/(e^{T_0/T} - 1)^2 \int_0^\infty dz[(e^z z)/(Ae^z + 1)^2]$, and $A = 1/(e^{T_0/T} - 1)$. The generation rate of electrons is given by Λ_{T_0}, and their initial injected energy per particle is $E_i = k_B T_i$. Figure 4 shows how electrons reach the lattice temperature at approximately 10 μm away from the filament centre for three different values of the electric current (three different generation rates Λ_0). The heating of the electron gas close to the filament increases with increasing generation rate.

3. Results and discussion

By applying equations (1)–(3), (9) and (13) we model the experimental results. In the experiments, a defocused uniform HeNe laser spot of diameter ∼600–700 μm was used and the spatially resolved photoluminescence from indirect excitons was collected [12]. According to the experimental data, the PL peak intensity profile exhibits a central dip surrounded by two maxima, indicating a ring ('Mexican hat') structure for the exciton distribution. The ring appears at around 10 μm from the anti-trap centre, and the ring formation is not affected too much by the laser power. This is consistent with our model which allows only well-thermalized electrons to form excitons and then recombine. The PL signal, which is attributed only to the ground-state excitons, is given by

$$I_{PL} = I_{PL}(r_\parallel) \sim N^x_{E=0}\frac{1}{\tau_R} \simeq \frac{T_0}{T}\frac{1}{\tau_R}, \tag{15}$$

where $N^x_{E=0} = e^{T_0/T} - 1$ is the occupation number of the ground-state mode, τ_R is the intrinsic radiative lifetime of indirect excitons and T_0 is the exciton degeneracy temperature. The concentration of excitons n^x_{2d} (note that $T_0 \sim n^x_{2d}$), calculated with the mass action law (9), is plotted in figure 4 against the in-plane radial distance $r_\parallel$. Because for $r_\parallel = 0$ the effective temperature $k_B T \sim E_b$, the excitons are partly ionized. This explains the nonmonotonic behaviour of $n^x_{2d} = n^x_{2d}(r_\parallel)$. In figure 5 we plot the spatial profile $I_{PL} = I_{PL}(r_\parallel)$ evaluated with equations (1)–(3), (9) and (13). Away from the ring position the PL signal decreases towards a small background level which depends upon the concentration of photogenerated carriers.

The calculated energy shift δE_x of the PL line, which is plotted in figure 6 against the radial distance $r_\parallel$ for four different intensities of the laser beam, again reproduces quantitatively the experimental data [12]. The bell-like shape is due to the accumulation of electrons injected from the filament.

The density of indirect excitons can be estimated from the energy shift and vice versa by using the plate capacitor formula $\delta E_x = 2\pi n^e_{2d} e^2 d/\varepsilon_b$, where d is the separation between electron and hole layers. Thus, the blue shift of the PL peak energy follows the change of the electron density $n^e_{2d} = n^e_{2d}(r_\parallel)$ around the centre of the filament. Away from the PLC the energy

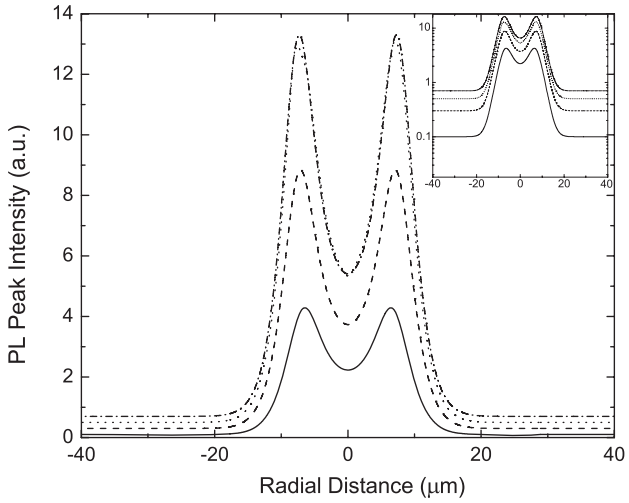

Figure 5. The PL peak intensity as a function of the radial distance from the anti-trap centre for four different laser powers. In the inset the same dependences are shown in a logarithmic scale. A ring structure appears around the anti-trap centre before the PL peak intensity reaches a background value. In our modelling we fit the experimental data for four different values of the laser power $P_{\text{laser}} = 25, 105, 550$ and 1660 μW (solid, dashed, dotted and dash–dotted lines, respectively).

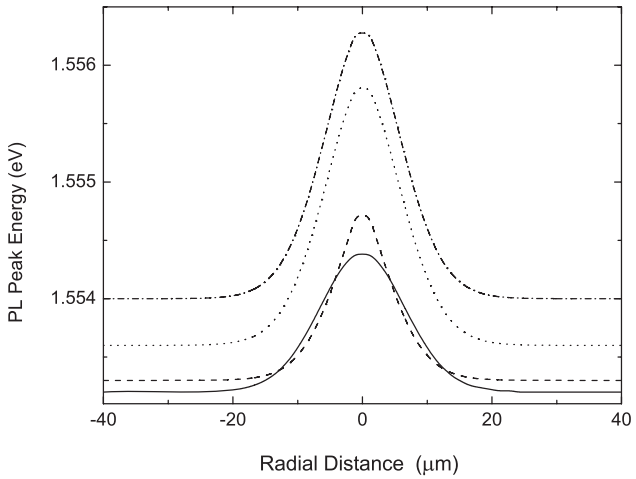

Figure 6. The peak energy of excitonic photoluminescence as a function of the radial distance from the anti-trap centre for four different laser powers as indicated in figure 5. The electron gas is hot near the anti-trap centre and its energy becomes constant away from it. The blue shift of the PL line with increasing laser power is clearly seen.

profile drops to a constant value which is higher for higher excitation powers. This background shift was initially attributed to a homogeneous background carrier distribution created under the uniform optical excitation. However, this is not consistent with the experimental results, which show a very low concentration not capable of reproducing such a large energy shift.

We explain such a behaviour in terms of device physics, considering the actual potential drop across the structure, U_{CQW}, as $U_{\text{CQW}} = U_{\text{Appl}} - RI$. Here, U_{Appl} is the applied voltage, $I = I_{\text{dark}} + I_{\text{pc}}$ is the total electric current across the structure (I_{dark} is the 'dark' current and

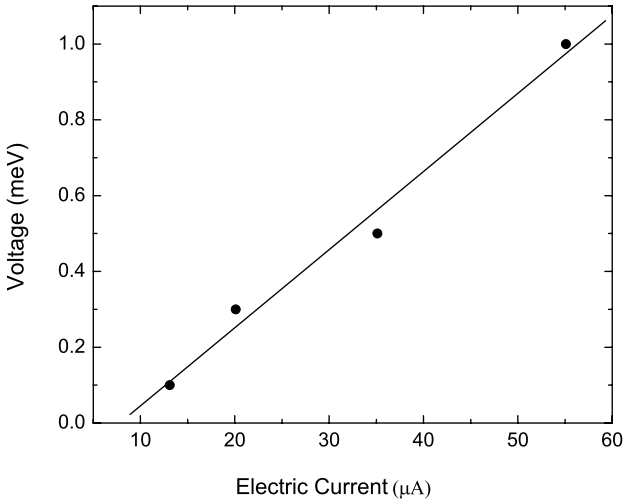

Figure 7. The voltage drop across the structure against the electric current. The blue shift scales linearly with the photocurrent, as is shown by the solid line, which is a fit to the measured points. The effective ohmic resistance, calculated as the gradient of the curve, is $R = 800\ \mathrm{k}\Omega$.

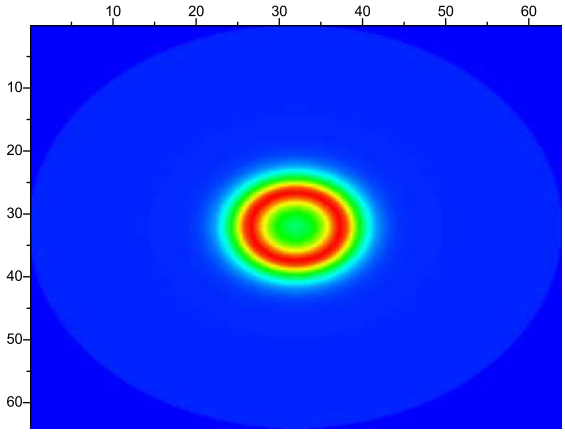

Figure 8. The PL signal plotted in the x–y plane. The grey (red online) colour refers to the highest intensity and the black (blue online) colour shows the background signal. A ring is formed around the centre of the filament at a distance of several micrometres.

(This figure is in colour only in the electronic version)

I_{pc} is the photocurrent), and R is the passive resistance of the whole electric circuit. With increasing optical intensity the photocurrent I_{pc} increases, causing a decrease of the actual potential drop U_{CQW}. The photoinduced change of U_{CQW} results in the change (blue shift) of the position of the energy E_{x}. In order to justify our explanation, in figure 7 we plot the experimentally observed background shift $\delta E_{\mathrm{x}}^{(0)}$ (the data are taken from [12]). The linear behaviour $\delta E_{\mathrm{x}}^{(0)} = \delta U_{\mathrm{CQW}}$, which corresponds to Ohm's law with $R = 800\ \mathrm{k}\Omega$, is clearly seen. Note that the inferred value of the resistance R is consistent with $R \sim 10^4$–$10^5\ \Omega$ measured in [12].

4. Conclusions

In this work we have studied the PL patterns of indirect excitons from the localized centres in double quantum well structures. The localized bright spots are attributed to defects in the nanostructure, where transverse current filaments cross the wells. The repulsive potential created in the vicinity of these anti-traps affects the in-plane carrier transport, which is simulated through the drift-diffusion model of equations (1) and (2). The charge density is calculated self-consistently using the three-dimensional Poisson's equation (3). After obtaining

the electron and hole concentration we apply the quantum mass action law, equation (9), to calculate the exciton concentration. The thermalization kinetics is given by equation (13), and it plays an important role in the explanation of the experimental data. The quantum-statistical corrections are included in our model. Application of this model to the experimental data reveals a quantitative agreement. In particular, the PL peak intensity exhibits a ring structure around the centre of the anti-trap (see figure 8) while the energy position of the PL line reaches a maximum at $r_{\parallel} = 0$. However, both the PL peak energy and intensity approach a constant value away from the anti-trap. We attribute the latter behaviour to the feedback current flowing through the device.

Generally, in experiments with a tightly focused laser excitation, excitons should be taken into account on an equal basis. Therefore an extra equation for excitons should be included in the drift-diffusion model in order to simulate the in-plane transport of all three species present in the structure, i.e. electrons, holes and excitons. This work is in progress and will be published elsewhere.

Acknowledgments

The authors would like to thank C W Lai for providing us with the experimental data, L E Smallwood for helping with the simulations and L V Butov for valuable discussions. Support of this work by the EU RTN Project HPRN-CT-2002-00298 'Photon-mediated phenomena in semiconductor nanostructures' is gratefully acknowledged.

References

[1] Butov L V, Gossard A C and Chemla D S 2002 *Nature* **418** 751
[2] Snoke D, Denev S, Liu Y, Pfeiffer L and West K 2002 *Nature* **418** 754
[3] Larionov A V, Timofeev V B, Hvam J and Soerensen K 2002 *JETP Lett.* **75** 200
[4] Butov L V, Levitov L S, Simons B D, Mintsev A V, Gossard A C and Chemla D S 2004 *Phys. Rev. Lett.* **92** 117404
[5] Rapaport R, Chen G, Snoke D, Simon S H, Pfeiffer L, West K, Liu Y and Denev S 2004 *Phys. Rev. Lett.* **92** 117405
[6] Kukushkin I V 2002 unpublished
[7] Butov L V 2004 *J. Phys.: Condens. Matter* **16** R1577
[8] Ivanov A L, Smalwood L E, Hammack A T, Yang S, Butov L V and Gossard A C 2006 *Europhys. Lett.* **73** 920
[9] Smallwood L E 2006 *PhD Thesis* Cardiff University, Cardiff, UK
[10] Butov L V, Lai C W, Ivanov A L, Gossard A C and Chemla D S 2002 *Nature* **417** 47
[11] Lai C W, Zoch J, Gossard A C and Chemla D S 2004 *Science* **303** 503
[12] Lai C W 2004 *PhD Thesis* University of California, Berkeley, USA
[13] Negoita V, Snoke D W and Eberl K 1999 *Phys. Rev.* B **60** 2661
[14] Hammack A T, Gippius N A, Yang S, Andreev G O, Butov L V, Hanson M and Gossard A C 2006 *J. Appl. Phys.* **99** 066104
[15] Hammack A T, Griswold M, Butov L V, Smallwood L E, Ivanov A L and Gossard A C 2006 *Phys. Rev. Lett.* **96** 227402
[16] Vörös Z, Snoke D W, Pfeiffer L and West K 2006 *Phys. Rev. Lett.* **97** 016803
[17] Gärtner A, Holleitner A W, Kotthaus J P and Schuh D 2006 *Appl. Phys. Lett.* **89** 052108
[18] Gorbunov A V and Timofeev V B 2006 *JETP Lett.* **83** 146
[19] de-Leon S B-T and Laikhtman B 2001 *Phys. Rev.* B **63** 125306
[20] Ivanov A L 2002 *Europhys. Lett.* **59** 586
[21] Ivanov A L 2004 *J. Phys.: Condens. Matter* **16** S3629
[22] Mouchliadis L and Ivanov A L 2007 unpublished
[23] Reinholz H 2002 *Solid State Commun.* **123** 489
[24] Szymanska M H and Littlewood P B 2003 *Phys. Rev.* B **67** 193305
[25] Ivanov A L, Littlewood P B and Haug H 1999 *Phys. Rev.* B **59** 5032